Interaction and Multiscale Mechanics, Vol. 1, No. 1 (2007) 157-175
DOI: http://dx.doi.org/10.12989/imm.2007.1.1.157

Ground vibrations due to underground trains considering soil-tunnel interaction

Y. B. Yang†

Department of Civil Engineering, National Taiwan University, No. 1, Section 4, Roosevelt Road, Taipei 10617, Taiwan

H. H. Hung‡

National Center for Research on Earthquake Engineering, Taipei 10688, Taiwan

L. C. Hsu‡†

Department of Civil Engineering, National Taiwan University, No. 1, Section 4, Roosevelt Road, Taipei 10617, Taiwan

(Received July 28, 2007, Accepted November 5, 2007)

Abstract. A brief review of the research works on ground vibrations caused by trains moving in underground tunnels is first given. Then, the finite/infinite element approach for simulating the soil-tunnel interaction system with semi-infinite domain is summarized. The tunnel is assumed to be embedded in a homogeneous half-space or stratified soil medium. The train moving underground is modeled as an infinite harmonic line load. Factors considered in the parametric studies include the soil stratum depth, damping ratio and shear modulus of the soil with or without tunnel, and the thickness of the tunnel lining. As far as ground vibration is concerned, the existence of a concrete tunnel may somewhat compensate for the loss due to excavation of the tunnel. For a soil stratum resting on a bedrock, the resonance peak and frequency of the ground vibrations caused by the underground load can be rather accurately predicted by ignoring the existence of the tunnel. Other important findings drawn from the parametric studies are given in the conclusion.

Keywords: ground vibration; infinite element; moving load; soil vibration; soil-tunnel interaction; subway; tunnel

1. Introduction

With the rapidly growing population in metropolitan areas, mass rapid transit systems built underground have emerged as an effective transportation tool for relieving the saturated ground traffic in different parts of the world. However, the vibration resulting from the trains moving underground, propagating through the soils to the ground, has sometimes reached the level which can hardly be tolerated by the neighboring residents. As such, the problem of train-induced

† Professor, Corresponding Author, E-mail: ybyang@ntu.edu.tw.
‡ Research Associate
‡† Former Graduate Student

vibrations has received increasing attention from both engineers and researchers. For example, a project named CONVURT (Clouteau 2005) was conducted by the European Union recently, aimed at controlling vibrations from underground rail traffic. Within the frame of this project, Chatterjee *et al*. (2003) and Degrande *et al*. (2006a) performed in-situ vibration measurements in Paris and London, respectively. Meanwhile, a periodic coupled finite element-boundary element formulation was proposed by Degrande *et al*. (2006b) for predicting free-field vibrations caused by metro trains moving through the tunnel. By considering the periodicity of the geometry in the longitudinal direction of the tunnel, the discretization of the elements is limited to a single-bounded cell.

Previous researches conducted along these lines can be generally classified into four categories as the *analytical approach*, *field measurement*, *empirical prediction models* and *numerical simulation*. A lot of researches on the ground-borne vibrations due to trains moving in underground tunnels were conducted by field measurement (Pan and Xie 1990) and empirical prediction models (Kurzweil 1979, Melke 1988, Trochides 1991, Hood *et al*. 1996), due to the fact that field measurement is the most reliable means for predicting absolute vibration levels in real situations and that empirical prediction models provide easier and cheaper ways for estimating the emission of vibration for underground railways in planning. However, neither of these approaches is suitable for the parametric study of different situations.

In contrast, analytical approaches can be employed to conduct a parametric study once the model is established. However, owing to existence of the tunnel structure and variations in soil layers, the classical elastic wave theory is not considered as an effective tool for treating the ground-borne vibrations associated with the underground railway traffic. Earlier related works performed by analytical approaches were usually conducted in the two-dimensional format, such as Balendra *et al*. (1991), Metrikine and Vrouwenvelder (2000), among others. Recently, Forrest and Hunt (2006a,b) proposed a three-dimensional analytical model for studying the train-induced ground vibration from a deep underground railway tunnel of circular cross-section. The tunnel is assumed to be an infinitely long, thin cylindrical shell, whereas the surrounding soil is modeled by means of the wave equations for an elastic continuum.

Concerning the vibrations due to trains moving in underground tunnels embedded by multi layers of soil deposits, numerical methods, such as finite element method, that are capable of simulating the tunnel structure and variations in soil layers appears to be most favored by engineers. However, traditional finite elements suffer from the drawback that the *geometric radiation effect* of the half space cannot be properly modeled. Thus, other schemes have to be incorporated to simulate such an effect. The *viscous boundaries* were used by Balendra *et al*. (1989) along with the finite elements to investigate the vibration of a subway-soil-building system in Singapore. Thiede and Natke (1991) used a similar scheme to study the influence of thickness variation of subway walls. Later, Chua *et al*. (1995) used a 2D finite-element idealization with the assumption of plain strain to reanalyze the same subway- soil-building system. The other popular scheme for modeling boundaries is the *boundary element method*. Andersen and Jones (2006) used coupled finite element-boundary element method to investigate the quality of the results gained from a two-dimensional model of a railway tunnel through comparison with those gained from a three-dimensional model. Degrande *et al*. (2006b) used a 3D periodic coupled finite element-boundary element formulation to study the dynamic interaction between a tunnel and a layered soil due to a harmonic excitation on the tunnel invert. In addition, Gardien and Stuit (2003) presented a *finite element based modular model* for predicting the vibrations induced by underground railway traffic. Such a model consists of three sub-models: the static deflection model, the track model and the propagation model. A parametric study was also performed to identify several factors that may affect the accuracy of the proposed method. Another scheme for simulating the semi-infinite boundary is the *infinite element method*, which has been successfully applied to problems related to ground vibration induced by traveling trains on the ground surface (Yang *et al*. 1996, Yang and Hung 2001).

From the review given above, we realize that the previous studies on ground-borne vibrations associated with the underground railway traffic are voluminous. However, most of these studies were performed for a specific case, rather than on the fundamental effects of soil and tunnel properties on ground vibrations. To fill such a gap, an extensive parametric study will be conducted in this paper to identify the key parameters that may affect the ground vibrations caused by trains moving through the underground tunnels.

Basically, there are three ways for modeling the half-space problems: three-dimensional (3D) modeling, 2D modeling, and 2.5D modeling. According to the research done by Andersen and Jones (2006) for 2D and 3D combined finite element and boundary element analyses for railway tunnel structures, although 3D models are required for absolute predictions, the two-dimensional model provides results that qualitatively agree with those of three-dimensional models at most frequencies. Consequently, for the soil-tunnel interaction problems of which the qualitative behavior, rather than the quantitative behavior, is of primary concern, a 2D model is considered sufficient. For the above reasons, as well as for the sake of reducing computational time, the *2D finite/infinite element approach* proposed by Yang *et al*. (1996) will be adopted to investigate the wave propagation behavior of a soil-tunnel interaction system due to trains moving in underground tunnels in the present study. With this approach, the soil-tunnel system is divided into two regions, i.e., the *near field* and *far field* (Fig. 1). The near field, including the loads and other geometric/material properties, is simulated by *finite (Q8) elements*, and the far field covering the soils with infinite boundary by *infinite elements*. By such a combination, the inherent drawback of the finite element method in simulating the radiation damping for waves traveling to infinity can be overcome. Moreover, the infinite elements can be easily incorporated in existing finite element programs for structures, which, therefore, is likely to be favored by most practicing engineers. Factors to be considered in the present parametric study include the soil stratum depth, damping ratio and shear modulus of the soil with or without the existence of a tunnel, and the properties and location of the tunnel structure. The results to be presented are the vibrations in frequency domain for different locations.

2. Problem formulation and basic assumptions

The problem to be considered is schematically shown in Fig. 1. The near field enclosing the

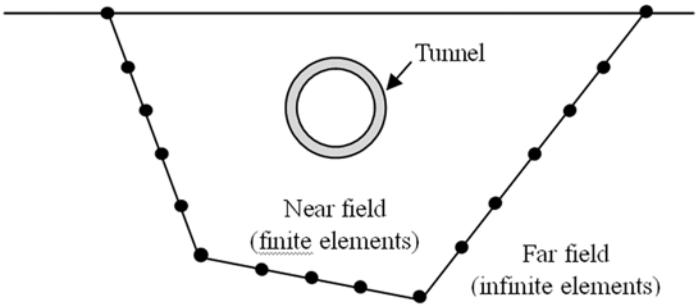

Fig. 1 Schematic of the finite/infinite element approach

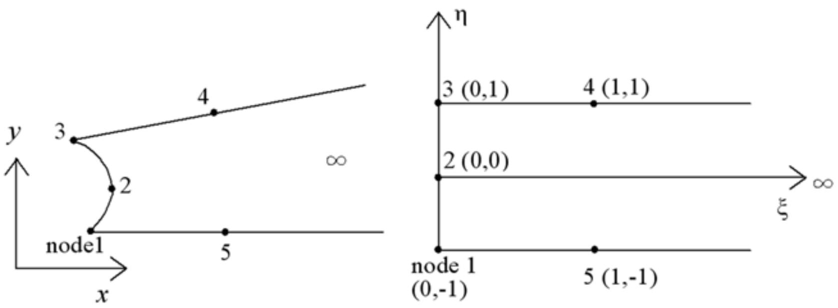

Fig. 2 Infinite element: (a) global coordinates, (b) local coordinates

tunnel is represented by finite elements, and the far field with infinity boundary by infinite elements to be summarized below. Plane strain conditions are assumed for the two-dimensional profile, and the train loads moving in the tunnel are modeled as harmonic line loads. Besides, hysteretic damping is assumed for the soil that is modeled as an isotropic viscoelastic medium.

Owing to the fact that finite elements are available in most textbooks, only the *infinite element* to be used will be summarized herein. The infinite element shown in Fig. 2 with the global coordinates (x, y) and local coordinates (ξ, η) can be regarded as a variant of the *quadratic 8-node (Q8) element*. The coordinates (x, y) of a point within the element can be related to those of the nodal points as:

$$x = \sum_{i=1}^{5} N_i' x_i, \quad y = \sum_{i=1}^{5} N_i' y_i \tag{1}$$

where the shape functions N' are assumed to be linear in ξ and quadratic in η, i.e.,

$$N_1' = -\frac{(\xi-1)(\eta-1)\eta}{2}, \quad N_2' = (\xi-1)(\eta-1)(\eta+1)$$
$$N_3' = -\frac{(\xi-1)(\eta+1)\eta}{2}, \quad N_4' = \frac{\xi(\eta+1)}{2}$$
$$N_5' = -\frac{\xi(\eta-1)}{2} \tag{2}$$

Similarly, the displacements (u, v) of a point within the element can be interpolated from the nodal displacements of the element as:

$$u = \sum_{i=1}^{3} N_i u_i, \quad v = \sum_{i=1}^{3} N_i v_i \tag{3}$$

where the shape functions N_i are

$$N_1 = \frac{\eta(\eta-1)}{2} \times P(\xi), \quad N_2 = -(\eta-1)(\eta+1) \times P(\xi)$$
$$N_3 = \frac{\eta(\eta+1)}{2} \times P(\xi) \tag{4}$$

The function $P(\xi)$ in Eq. (4) is known as the *propagation function*,

$$P(\xi) = \exp(-\alpha_L \xi) \times \exp(-ik_L \xi) \tag{5}$$

where α_L denotes the *displacement amplitude decay factor* to account for the geometric attenuation, and k_L the *wave number* of the waves traveling outward.

The propagation function $P(\xi)$ is the quintessence of infinite element, which allows the wave to travel through the boundary and decay geometrically. Some guidelines for determining the wave number k_L and the amplitude decay factor α_L for infinite elements located in different regions of the half space under different types of loadings, as well as the dynamic condensation procedure that makes the finite/infinite element mesh frequency-independent, are available in Yang *et al*. (1996).

By assuming both the loading and displacement to be of the harmonic type, one can derive the equation of motion for the finite/infinite element system under a particular excitation frequency ω as

$$(-\omega^2[M]+[K])\{\Delta\} = \{F\} \tag{6}$$

where $\{\Delta\}$ and $\{F\}$ denote the amplitudes of the nodal displacements and applied loads, respectively, and $[M]$ and $[K]$ are the stiffness and mass matrices of the system. As was stated previously, the near field of the half space, including the tunnel structure, is modeled by the finite (Q8) elements and the far field with infinite domain by the infinite elements. By the conditions of compatibility and equilibrium at the nodal points of the system, the mass and stiffness matrices for all the finite and infinite elements can be assembled to form the structural matrices and thus the equations of motion for the entire soil-tunnel system can be established and solved.

3. Basic considerations in parametric studies

In our analysis, a unit harmonic line load $\exp(i\omega t)$ will be applied at a certain depth below the surface to simulate the action of the moving train. With the finite/infinite method described, the influence of varying parameters upon the vibration of soils and tunnel will be studied. To focus on the effect of the tunnel structure, two structural configurations will be considered, namely, a half space without a tunnel (Fig. 3a), and a half space with a circular tunnel of concrete lining (Fig. 3b). Later, a third configuration will be added by letting the tunnel consist of material same as the surrounding soil, resulting in the so-called “circular hole”. For each configuration, two different soil conditions will be considered, i.e., a homogeneous half-space and a soil deposit overlying an elastic half-space or a bedrock.

The properties adopted for the top soil layer of both structural configurations are: elastic modulus $E_s = 3\times10^7$ N/m^2, Poisson’s ratio $\upsilon = 0.3$, density $\rho = 1{,}900$ kg/m^3, and material damping ratio $\beta = 0.05$. Accordingly, the shear wave velocity of the soil is $C_s = 77.93$ m/s, and the compressional wave velocity

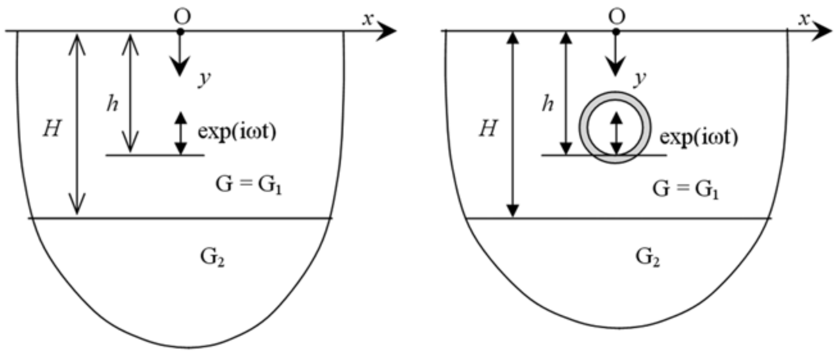

Fig. 3 Schematic of problem: (a) with no tunnel, (b) with a tunnel

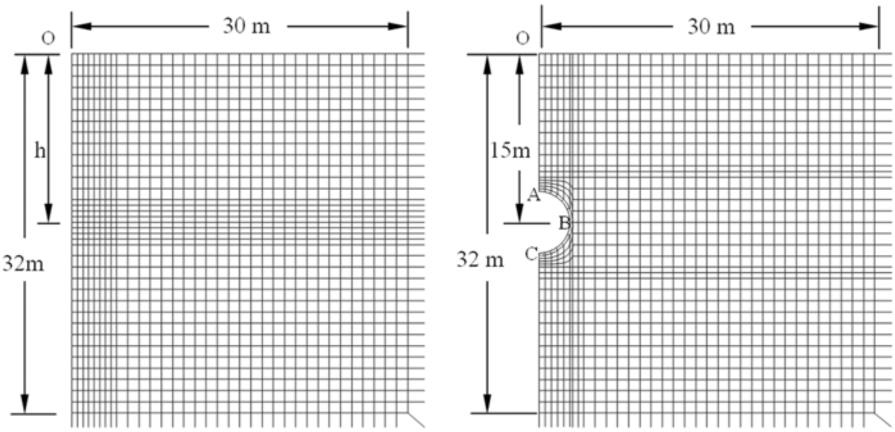

Fig. 4 Finite and infinite element mesh: (a) with no tunnel, (b) with tunnel

is $C_p = 145.79$ m/s. For the configuration in Fig. 3(b), the material properties of the concrete tunnel lining are: elastic modulus $E_c = 2.5 \times 10^{10}$ N/m^2, Poisson's ratio $\upsilon_c = 0.2$, density $\rho_c = 2{,}400$ kg/m^3, and material damping ratio $\beta_c = 0.02$. The centroid of the tunnel is 15 m below the ground surface. The inner diameter of the tunnel is 5.5 m and the thickness of the tunnel lining is 0.25 m. The properties of the soil and tunnel adopted herein are obtained from one site of the Taipei MRT System.

The mesh to be used in this paper is shown in Fig. 4, in which only half of the system (width = 30 m, depth = 32 m) is modeled due to symmetry. The far field is modeled by infinite elements and the near field by Q8 elements. The element sizes shown in Fig. 4 were generated to meet the requirements for simulating the highest frequency of loading considered (20 Hz), namely, the *maximum element size* (L) and *minimum mesh extent* (R) were selected such that $L \le \lambda_s / 6$ and R $\;0.5\lambda_s$, where λ_s is the shear wave length of soil corresponding to the highest frequency considered (Yang *et al*. 1996). In terms of the accuracy and efficiency of computation, modeling with such meshes appears to be most economic, which thus will be adopted throughout the numerical studies. Since the vertical displacements are much higher than the horizontal displacements for most cases studied, only the vertical displacements V will be presented, which will be multiplied by the shear modulus G of the soil to make the results independent of the latter. The frequency range considered in current study is from 0 to 20 Hz because for vibrations with frequencies higher than 20 Hz, their high attenuation rate will make their amplitudes on the far-field ground surface negligible as compared with those of lower frequencies. However, the results to be presented may cover a range of frequencies smaller than 20 Hz to make the graphs more legible.

4. Ground vibrations due to an underground line load

The first problem considered is an elastic half-space subjected to a unit harmonic line load $\exp(i\omega t)$ acting at a depth h (m) from the surface as shown in Fig. 3(a).

4.1 Effect of loading depths for homogeneous elastic half-space

The vertical displacements of various points on the ground surface due to different loading depths

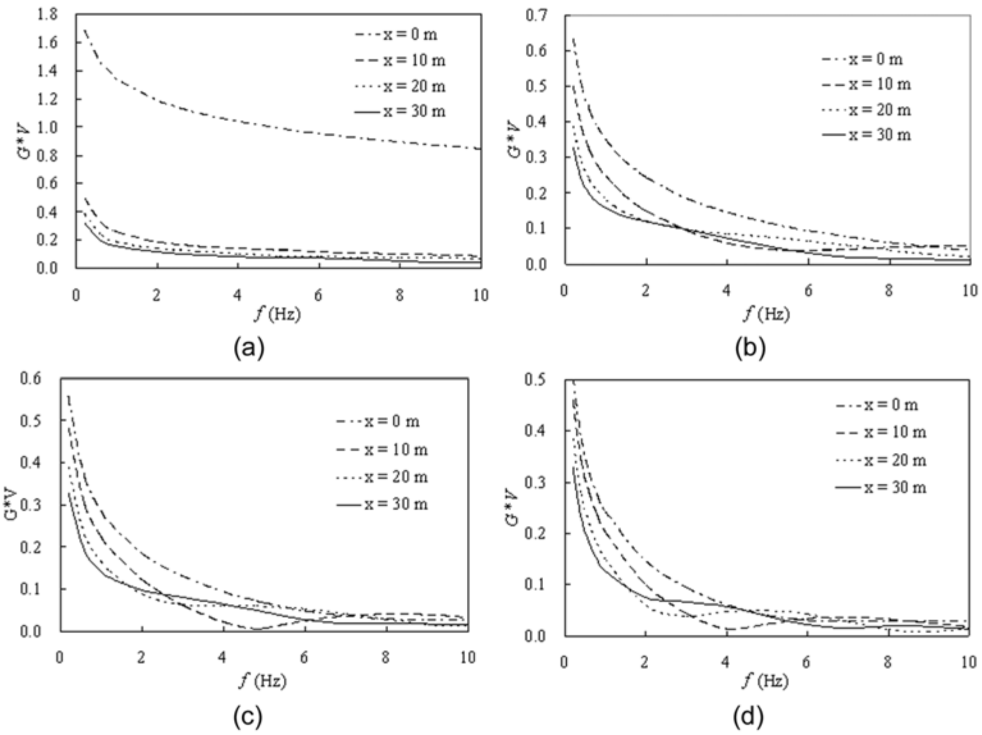

Fig. 5 Vertical displacements of ground surface for various loading depths (homogeneous half-space) for: (a) $h = 0$ m, (b) $h = 10$ m, (c) $h = 15$ m, (d) $h = 20$ m

were first conducted. Fig. 5 shows the responses for various observation points on the ground surface vs. the excitation frequency $f = \omega / 2\pi$ of the harmonic line load applied at different depths h. As can be seen, for the case with the load applied on the ground surface ($h = 0$ m), as indicated by Fig. 5(a), *larger decaying rate can be observed for observation points closer to the source.* For the cases with the load applied underground ($h > 0$), *the decaying rate of the maximum ground displacement at each point becomes generally mild.* In addition, some higher frequency vibrations can be observed for farther observation points, especially for larger loading depths h. As such, for the case with $h > 0$, the increase in distance x does not always lead to a decrease in the vibration amplitude for some frequencies. The other observation is that when the loading is located at $h = 10$ m below the ground surface, the amplitude of the response at the origin reduces by more than 50%, compared with the case where the load is applied at the origin, as revealed by Figs. 5(a) and (b). Further increase in the depth of the loading point results only in slight difference in the surface response, as can be seen from Figs. 5(b)-(d).

The frequency contents at the origin and loading point for different depths of loading were plotted in Figs. 6(a) and (b), respectively. From Fig. 6(a), we observe that *the response amplitude decreases with the increase in the depth of loading for frequencies less than 6 Hz.* For frequencies higher than 6 Hz, the response is rather insensitive to the variation in the depth h of loading. For the responses at the loading point, as indicated by Fig. 6(b), a clear *resonance frequency* can be observed for the case with $h > 0$, and *the resonance frequency decreases as the loading depth h increases.*

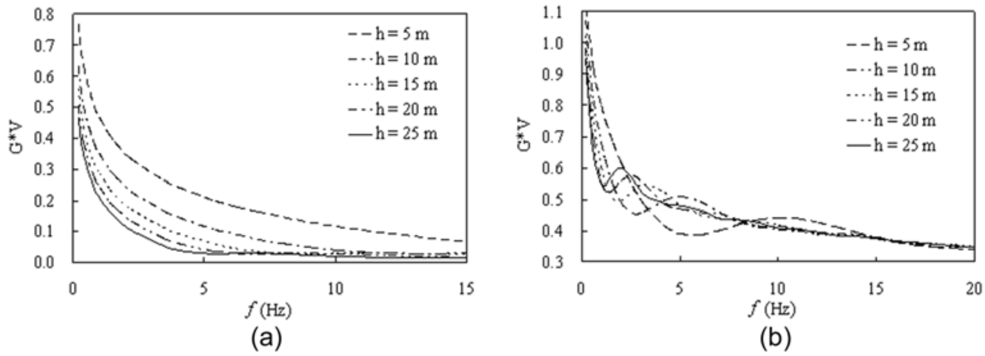

Fig. 6 Vertical displacements of soils due to loads acting at various depths (homogeneous half-space): (a) at origin O, (b) at the loading point

4.2 Effect of shear modulus ratio of soil layers

Consider the case of a soil layer with thickness $H = 30$ m and shear modulus G_1 superposed on an elastic half space with shear modulus G_2, where G_1 is calculated from the standard soil properties given previously. Assume that the load is applied at a depth of $h = 15$ m. The surface responses computed for the origin O and a point with distance $x = 30$ m have been plotted in Figs. 7(a) and (b), respectively, for different shear modulus ratios: $G_1/G_2 = 1.0$, 0.5, 0.25, 0.05, 0.0, where the condition $G_1/G_2 = 0$ implies that a soil layer is deposited on the top of the *bedrock*, and the condition $G_1/G_2 = 1$, a *homogeneous half space*. The other conditions with $G_1/G_2 < 1$ imply that the upper layer soil is softer than the lower one. The results indicate that there is no resonance for the homogeneous case ($G_1/G_2 = 1$), but some *resonance* takes place as the shear modulus ratio G_1/G_2 decreases and approaches zero.

The above phenomenon can be explained as follows. For the case with a bedrock, incident body waves (i.e., compressional waves and shear waves) will be reflected by the rock surface. As a result, *resonance occurs when the frequency of the soil layer equals that of the excitational force*. According to Wolf (1985), for a single homogeneous soil layer, the *resonance frequency* of the

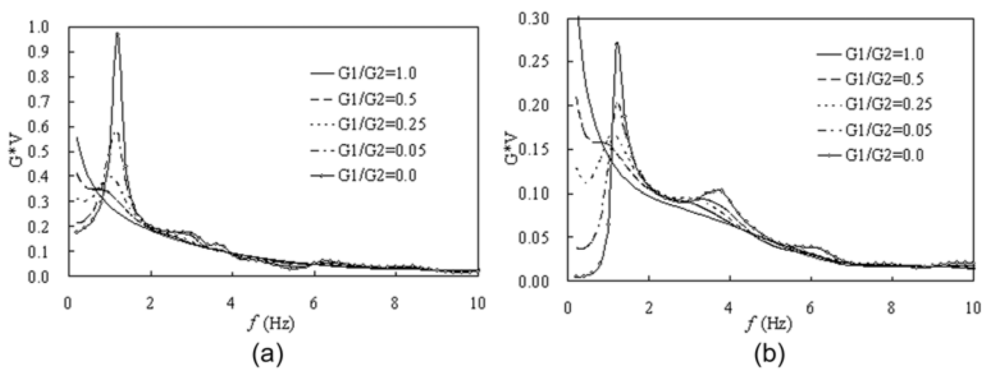

Fig. 7 Vertical displacements of surface points vs. shear modulus ratio of soil layer (h = 15 m): (a) at origin O, (b) at $x = 30$ m

vertical incident *compressional waves* is:

$$f_p = (2n-1)\frac{C_p}{4H} \tag{8}$$

and the resonance frequency of the vertical incident *shear waves* is:

$$f_s = (2n-1)\frac{C_s}{4H} \tag{9}$$

where C_s and C_p denote the velocities of the shear waves and compressional waves, respectively, and H is the thickness of the soil layer. The vertical vibration concerned herein results mainly from the compressional waves, for which the resonance frequency should be slightly smaller than f_p and greater than f_s. As shown in Fig. 7(a) for the origin, the primary resonance frequency for the case $G_1/G_2 = 0$ is about 1.2 Hz, which is close to the value predicted using Eq. (8) by letting $n = 1$. Although a secondary resonance can be observed for the frequency near 3.6 Hz, the resonance peak is rather small compared with the primary resonance peak. *For observation points with larger distances,* e.g., for $x = 30$ m as shown in Fig. 7(b), *the cutoff frequency of 1.2 Hz can be clearly observed*, i.e., no waves with a frequency lower than 1.2 Hz can propagate outward to such a distance as x = 30 m for the case with a bedrock ($G_1/G_2 = 0.0$). Other resonance frequencies around 3.6 Hz and 6 Hz can also be clearly observed from Fig.7 (b).

Another observation from Fig. 7 is that *resonance becomes more pronounced as the shear modulus ratio G_1/G_2 decreases, as indicated by the increasing peak amplitude*. This is due to the difference in the energy proportions of refracting and reflecting waves on the interface caused by impedance mismatch of adjacent soil layers. For the case with $G_1/G_2 = 0.0$, the peak amplitude reaches the highest due to total reflection.

4.3 Effect of loading depth for the case of a soil layer resting on a bedrock

For a soil stratum of thickness $H = 30$ m, Figs. 8 (a)-(d) show the surface displacements for different loading depths h. Except for the occurrence of the first resonance frequency, the trend of variation of the surface displacement is similar to that for the homogeneous half space in Fig. 5. *For the loading point located beneath the surface, some higher frequencies of vibration can be observed for points of observation with larger distances*, i.e., with larger x. Besides, an increase in the loading depth makes the higher mode resonance frequency of the soil layer more visible. The same phenomena can also be observed from Fig. 9, which shows the frequency content at the origin and at the loading point for the different depths of loading. As can be seen, the first resonance *peak of the soil layer decreases dramatically as the loading depth increases*, for both the origin and the loading point. On the contrary, as the loading gets deeper, the amplitude for the higher frequencies becomes more significant compared with that of the first peak. The difference in resonance peaks for different loading points can be partly attributed to the fact that the loading applied at certain depths may activate soil layer vibration of some specific frequencies easier than the others.

4.4 Effect of depth of soil stratum

Consider the case where the load is applied at the depth of $h = 15$ m, but with different depths H for the underlying rock. The maximum surface displacements computed have been plotted with

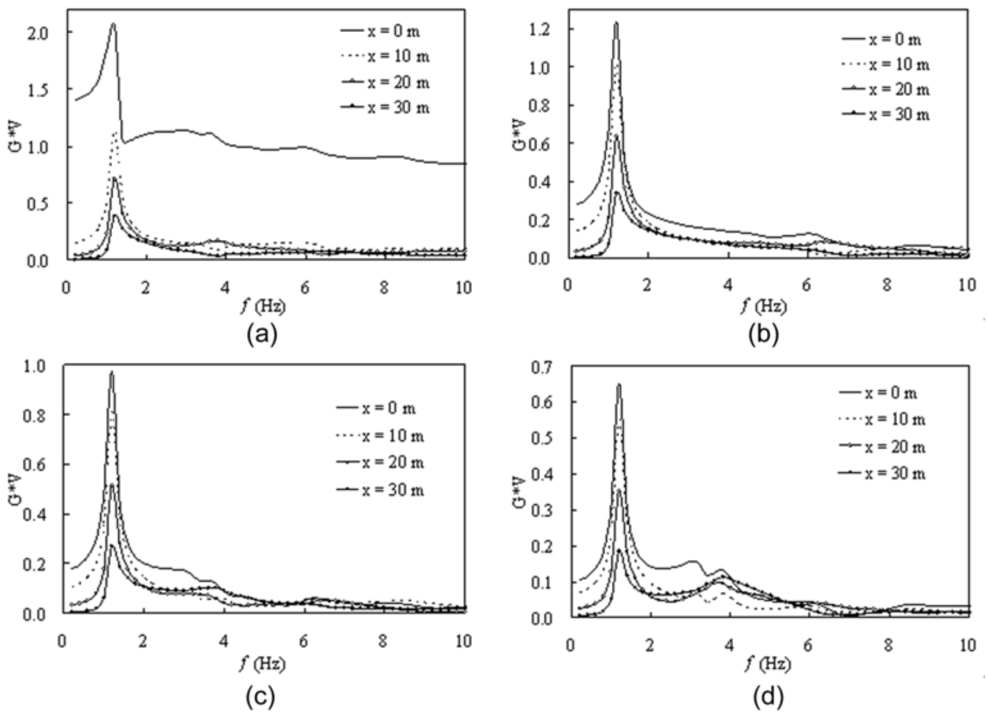

Fig. 8 Vertical displacements of ground surface for various loading depths (stratum thickness $H = 30$ m) for: (a) $h = 0$ m, (b) $h = 10$ m, (c) $h = 15$ m, (d) $h = 20$ m

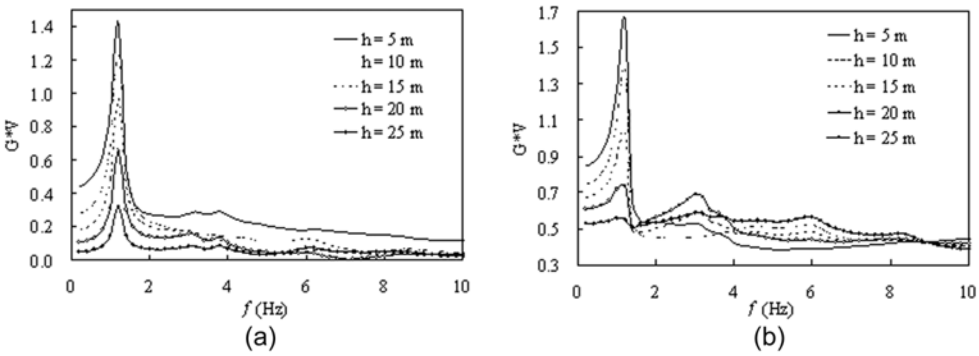

Fig. 9 Vertical displacements of soils due to loads acting at various depths (stratum thickness H = 30 m): (a) at origin O, (b) at the loading point

respect to the frequency for different depths H and different surface points x in Figs. 10. As can be seen, *a deeper bedrock is accompanied by a smaller resonance frequency, but a larger peak.* Moreover, *the resonance frequency of each point on ground surface is the same for the bedrock of the same depth*. For the current case with $h =$ 15 m, the primary resonance frequencies computed from Eq. (8) for $H = 20$, 25, and 30 m are 1.8, 1.5, and 1.2 Hz, respectively, in close agreement with those shown in Fig. 10. Another observation from Fig. 10 is that although the primary resonance peak increases slightly as the rock depth increases, the secondary resonance frequency becomes less visible. Besides, for an observation point at a larger distance, e.g., for $x = 30$ m as

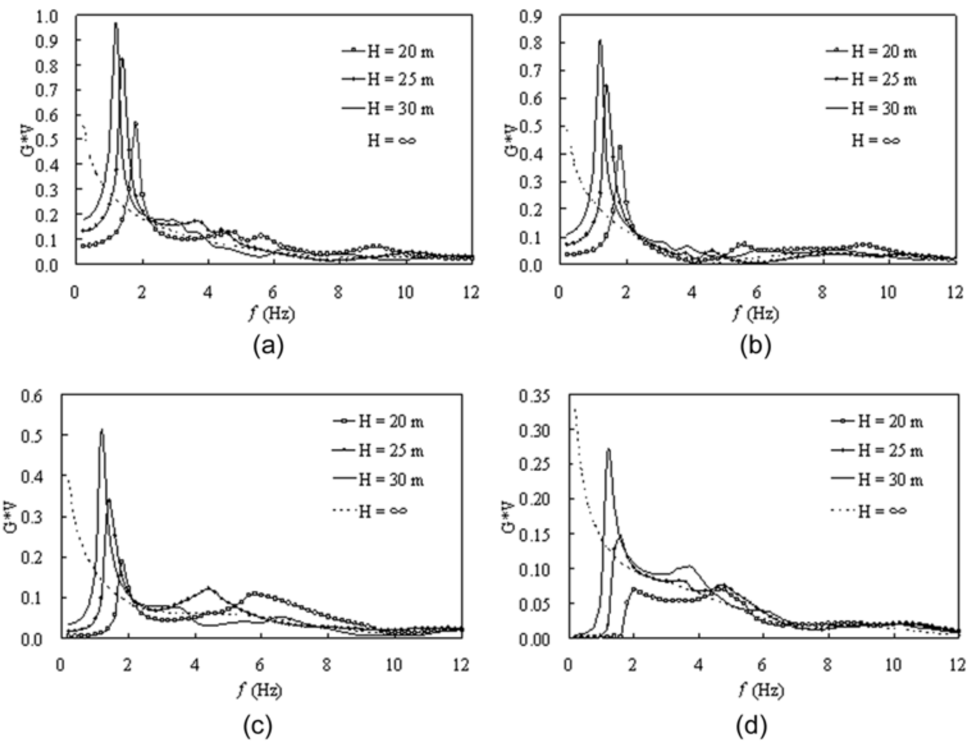

Fig. 10 Vertical displacements of surface points for soil strata of various thicknesses: (a) at origin O, (b) at x = 10 m, (c) at x = 20 m, (d) at x = 30 m

shown in Fig. 10(d), the responses for the frequencies less than the first resonance frequency or cutoff frequency become insignificant.

4.5 Effect of soil damping ratio

With the load applied at the depth of $h = 15$ m, Figs. 11 and 12 show the effect of the soil damping ratio on the surface displacement for a soil deposit overlying the bedrock ($H = 30$ m) and homogeneous half-space, respectively. *For the case of a bedrock* (Fig. 11), *a larger soil damping ratio is accompanied by a smaller peak*, but no change in the resonance frequency. Meanwhile, the resonance frequencies predicted by Eq. (8) for $n = 1$ to 8 can all be observed from Fig. 11 for the case of zero damping. *For the case of homogeneous half-space* (Fig. 12), *no resonance frequency is observed for the soil*, but a larger damping ratio generally results in a smaller response. Another phenomenon to be noted in Fig. 12 is that although no natural frequency exists for a homogeneous half-space, some peaks can still be observed in Fig. 12, especially for the case at $x = 20$ m and of zero damping.

5. Ground vibrations due to a line load acting in a tunnel

Consider the 2D soil-tunnel profile subjected to a unit harmonic line load $\exp(i\omega t)$ at the bottom central point of the tunnel, which has a depth h from the ground surface (Fig. 3b).

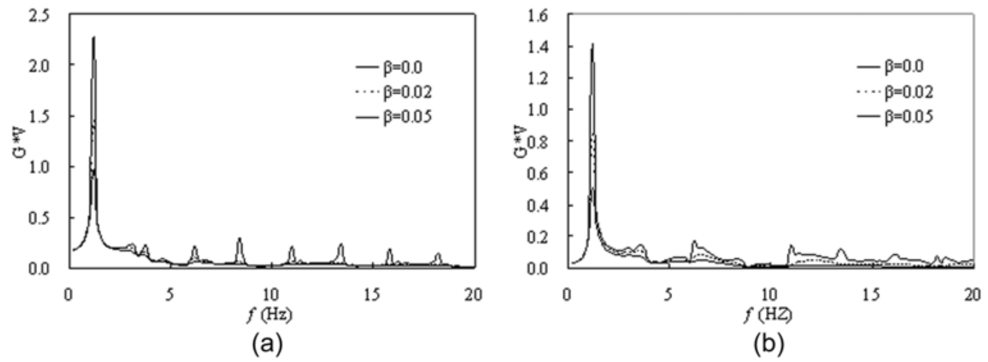

Fig. 11 Vertical displacements of surface points for various damping ratios (stratum thickness $H = 30$ m): (a) at origin O, (b) at $x = 20$ m

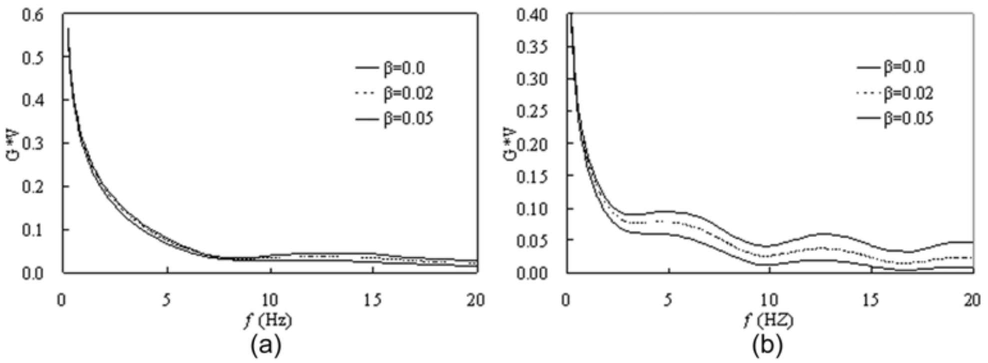

Fig. 12 Vertical displacements of surface points for various damping ratios (homogeneous half-space): (a) at origin O, (b) at $x = 20$ m

5.1 Effect of existence of tunnel structure

The effect of tunnel structure on the ground vibrations will be investigated for the two cases: (a) a homo-geneous half-space and (b) a soil layer overlying a bedrock. Three different configurations are considered, i.e., without a tunnel (Fig. 3a), with a circular tunnel of a 5.5 m internal radius with concrete lining (Fig. 3b), and with a circular tunnel of 5.5 m internal radius but no concrete lining (referred to as a "circular hole"). For all these configurations, a unit harmonic line load is applied at a depth of $h = 17.75$ m below the ground surface. The analysis results for a homogeneous half-space and a soil layer with thickness $H = 30$ m overlying the bedrock are shown in Figs. 13 and 14, respectively, where parts (a) to (c) show the results for three surface points and part (d) the loading point.

For both the homogeneous half space and a soil layer overlying the bedrock, only *slight difference* can be observed for the surface displacements between the configurations of a circular tunnel and no tunnel, but for the loading point, the displacement amplitudes for the configuration with tunnel are much lower than that for the case with no tunnel. This reason for the similar surface responses observed for both configurations with and without tunnel is that *the stiffness of the tunnel lining somehow compensates for the loss of stiffness due to excavation of the circular hole.*

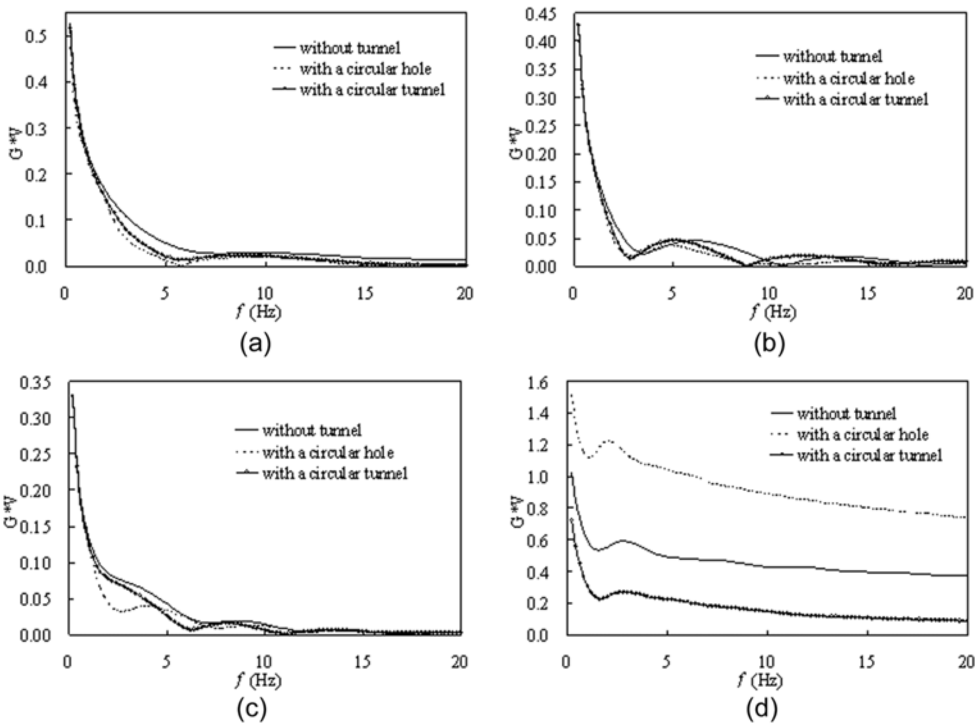

Fig. 13 Vertical displacements for various structural configurations (homogeneous half-space): (a) at origin O, (b) at $x = 15$ m, $y = 0$ m, (c) at $x = 30$ m, $y = 0$ m, (d) at the loading point ($x = 0$ m, $y = 17.75$ m)

Concerning the effect of *circular hole*, for the homogeneous half space the existence of a circular hole does not change the surface responses significantly (Fig. 13), However, for the case with a bedrock (Fig. 14), the primary resonance peak of the surface displacement for the configuration with a circular hole is much less than that with no tunnel. On the contrary, the displacement amplitude at the loading point for the configuration with a circular hole is much higher than the other two configurations.

By comparing the vertical displacements at different points inside the tunnel, as indicated in Fig. 4(b), with that of the origin O in Fig. 15, the effect of the concrete tunnel becomes obvious. For the case with a bedrock, as shown in Fig. 15(b), the response at the bottom C of the tunnel is drastically amplified at the second resonance frequency near 3.6 Hz, compared with that at the origin O. The response at Point B inside the tunnel also has a similar trend, but with a smaller amplitude. Unlike Points B and C, the response at Point A (i.e. top of the tunnel) is generally similar to that at the origin O.

5.2 Effect of thickness of tunnel walls

By varying the thickness of concrete lining of the tunnel, the vertical displacements of Points O, A, B and C are plotted in Figs. 16 (a)-(d), respectively. Obviously, the effect of thickness of tunnel walls is drastically different for different observation points. For instance, for Points O (origin) and A (top of tunnel), the increase in tunnel thickness will result in increase of the amplitude of vertical

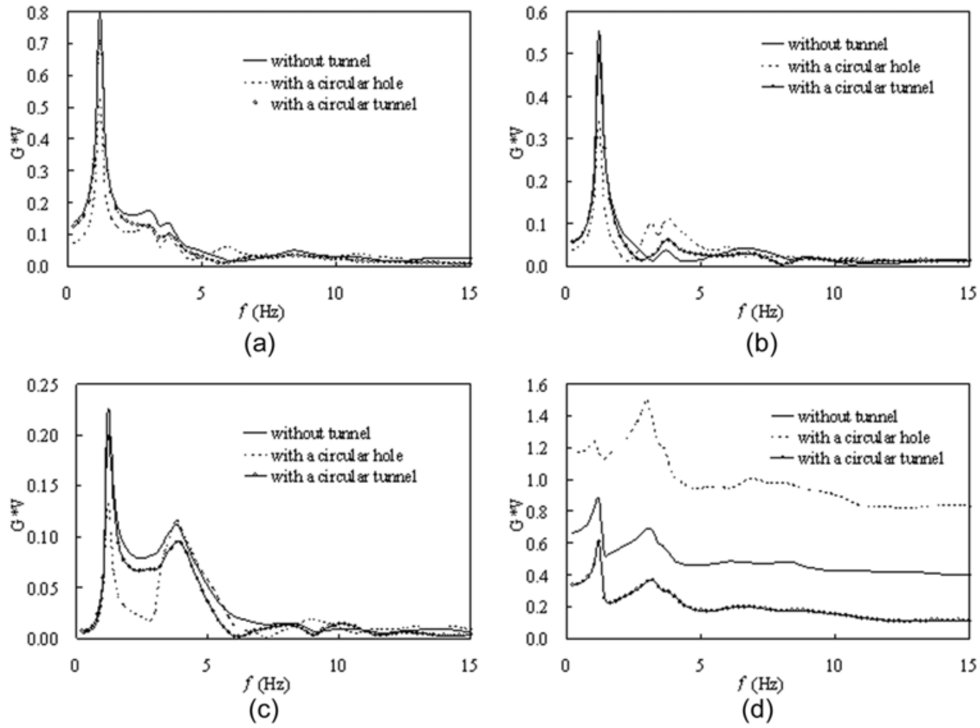

Fig. 14 Vertical displacements for various structural configurations (stratum thickness $H = 30$m): (a) at origin O, (b) at $x = 15$ m, $y = 0$ m, (c) at $x = 30$ m, $y = 0$ m, (d) at the loading point ($x = 0$ m, $y = 17.75$ m)

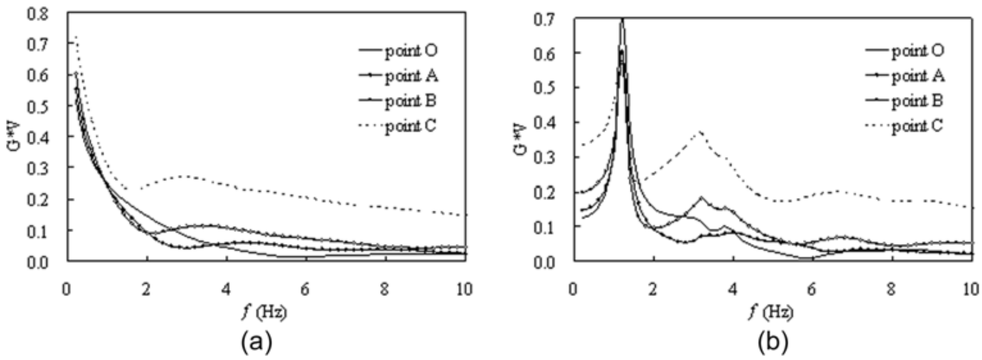

Fig. 15 Vertical displacements of various observation points: (a) homogeneous half-space, (b) stratum thickness $H = 30$ m

displacement. However, for Point C (bottom of tunnel), the increase in tunnel thickness is accompanied by a rather large reduction in displace-ment amplitude. For Point B (side of tunnel), the first resonance peak increases with an increase in the tunnel thickness, while for the second resonance peak, the reverse is true.

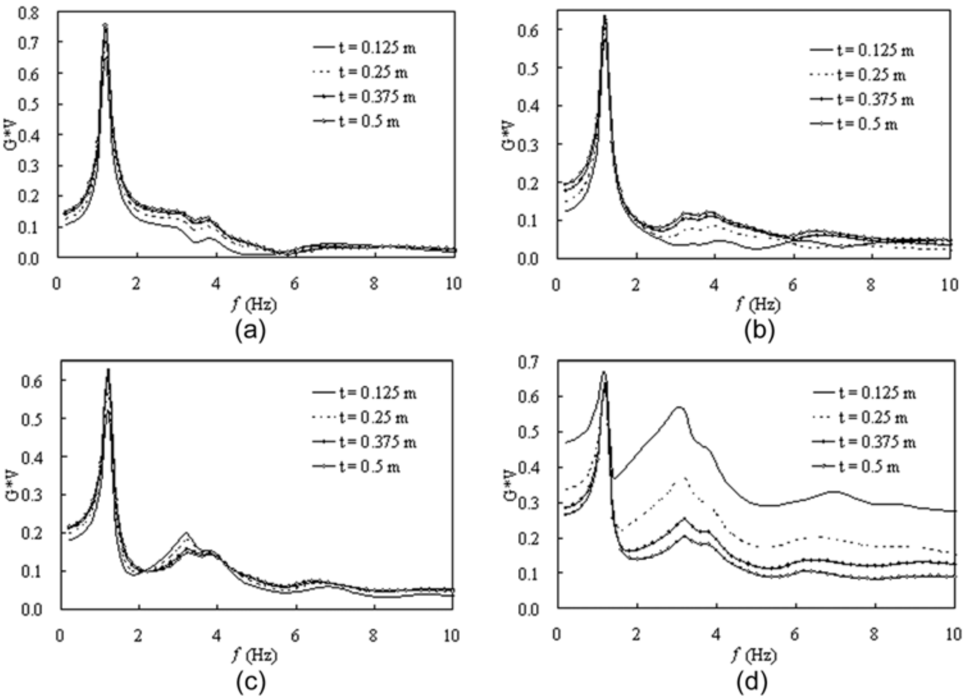

Fig. 16 Vertical displacements of different observation points for various tunnel thicknesses at: (a) origin O, (b) Point A, (c) Point B, (d) Point C

5.3 Effect of shear modulus ratio of soil layers

Consider the case of a soil layer with thickness $H = 30$ m and shear modulus G_1 superposed on an elastic half space with shear modulus G_2 as shown in Fig. 3(b). The vertical responses computed for the ground surface at the origin O and at loading point (Point C) inside the tunnel have been plotted in Figs. 17(a) and (b), respectively, for different shear modulus ratios. Again, the condition $G_1/G_2 = 0$ implies a soil layer deposited over a bedrock, and the condition $G_1/G_2 = 1$, a homogeneous half space. The other conditions with $G_1/G_2 < 1$ imply softer upper layers.

Similar to the trend observed on Fig. 7(a) for the case with no tunnel, Fig. 17(a) reveals that no resonance is observed at the origin O for the homogeneous case, i.e., with $G_1/G_2 = 1$, but *as the shear modulus ratio G_1/G_2 decreases and approaches zero, some resonance peaks may occur.* Similar phenomenon occurs at Point *C*, namely, the resonance is not obvious for the homogeneous case with $G_1/G_2 = 1$. But as the shear modulus ratio G_1/G_2 decreases and approaches zero, meaning that the upper soil layer is getting softer than the lower one, both the first and second resonances become more pronounced.

5.4 Effect of depth of bedrock

Let us investigate the effect of depth *H* of the bedrock. From Fig. 18, we observe that for both the origin O and at distance of $x = 20$ on the ground surface, *the primary resonance peak increases as the bedrock depth H increases*, and the resonance frequencies are in consistent with that shown in

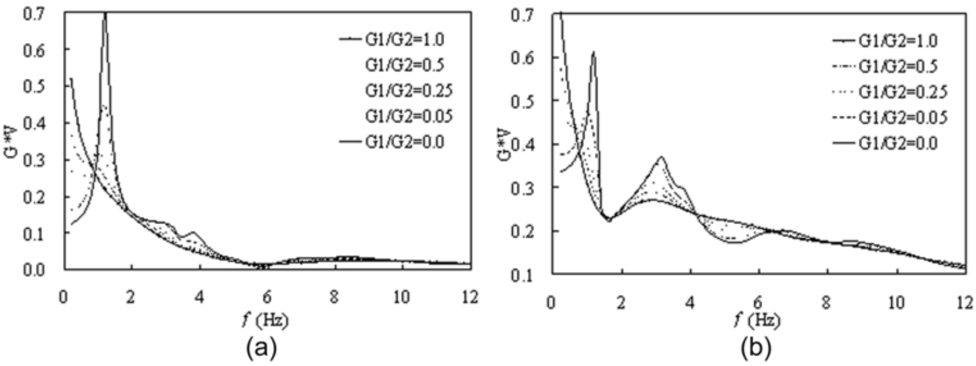

Fig. 17 Vertical displacements of different observation points for various shear modulus ratio of soils: (a) at origin O, (b) at Point C

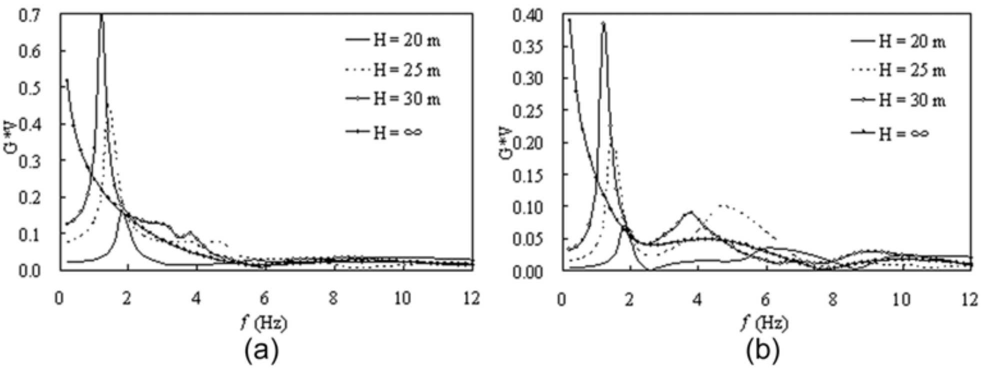

Fig. 18 Vertical displacements of different observation points for bedrock of various depths: (a) at origin O, (b) at $x = 20$ m, $y = 0$ m

Fig. 10. Another observation Fig. 18(b) is that as the rock depth decreases, the second resonance peak becomes more visible.

5.5 Effect of elastic modulus ratio of soil/tunnel

Let us focus on the relative hardness of the soil with respect to the tunnel structure. Again, a soil stratum of thickness $H = 30$ m lying on the bedrock is assumed. The properties of the tunnel section are the same as those used previously. Three elastic modulus ratios E_s/E_c are considered for the soil relative to the concrete tunnel: 0.001, 0.005 and 0.01. By selecting the elastic modulus of the concrete tunnel E_c as 2.5×10^{10} N/m^2, the elastic modulus of the soil E_s is found as 2.5×10^7, 1.25×10^8, 2.5×10^8 N/m^2. Correspondingly, the speeds of compressional waves are 133.1, 297.6 and 420.9 m/s, and the primary resonance frequencies computed from Eq. (8) are 1.11, 2.48 and 3.51 Hz, respectively.

As can be seen from Fig. 19, the *primary resonance frequency* of the soil layer for both the origin O and at Point with $x = 20$ m corresponds very well to those predicted by Eq. (8), which *increases as the soil elastic modulus increases*. Noteworthy herein is the fact that the responses shown in Fig. 19 have been multiplied by the shear modulus G of the soil layer, so that the real responses for soil

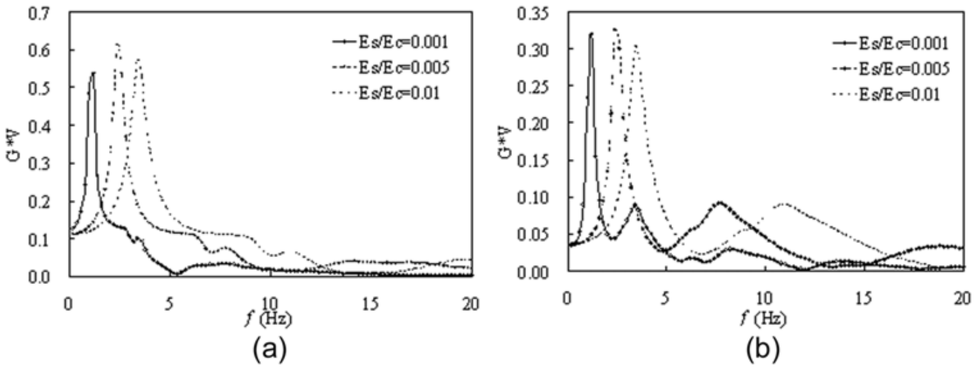

Fig. 19 Vertical displacements of different observation points for various elastic modulus ratios (with $H = 30$ m): (a) at origin O, (b) at $x = 20$ m

with lower value of elastic modulus ratio, e.g., $E_s/E_c = 0.001$, are higher than that of $E_s/E_c = 0.01$ by ten times roughly. Therefore, the elastic modulus ratio of soil is the key factor for the absolute value of the response, i.e., higher ground vibrations will be induced by softer soil layers.

6. Concluding remarks

In this paper, the finite/infinite element approach has been employed to investigate the vibration of a soil-tunnel interaction system induced by a harmonic line load on the tunnel. From the parametric study, we found that the vibrations on the ground surface mainly depend on the soil properties and the tunnel depth. However, the responses on the tunnel structure will depend highly on the tunnel properties. Other observations are summarized in the following. The conclusions drawn below remain strictly valid for the conditions assumed in the analysis:

6.1 Ground vibrations due to an underground line load (without tunnel)

a - For a homogeneous half space or for a soil stratum overlying a bedrock under a harmonic line load on the ground (with $h = 0$ m), the maximum ground displacement decays dramatically with increasing distance from the source. Larger decaying rate can be observed for observation points closer to the source. However, when the loading point is located under the ground surface, the decaying rate of the maximum displacement along ground surface becomes generally mild. Moreover, as the depth of the loading point increases, vibrations of higher frequencies will be induced.

b - For a soil layer lying on a bedrock, the incident body waves (compressional waves and shear waves) will be reflected when reaching the rock surface. Thus, resonance occurs when the frequency of the soil layer equals that of the applied load, and larger peaks are observed for softer soil layers. A deeper bedrock will result in a smaller resonance frequency, but a larger peak value. The resonance frequency of each point on the ground remains basically the same as long as the depth of bedrock is the same.

c - For a homogeneous half space, a resonance frequency can be observed at the loading point, which decreases as the depth of the applied load increases. For a soil layer lying on a bedrock, the first resonance peak of the soil decreases as the loading depth increases, and the higher resonance frequencies become more visible at the loading point as the loading depth increases.

d - For a soil layer lying on a bedrock, the resonance peak decreases as damping ratio of the soil increases.

6.2 Ground vibrations due to a line load acting in a tunnel

a - As far as ground vibration is concerned, the existence of a concrete tunnel may somehow compensate for the loss due to excavation of the tunnel. Only slight difference can be observed for the cases with and without tunnel.

b - The effect of tunnel thickness is drastically different for different observation points. At the ground surface and tunnel apex, the increase in tunnel thickness will result in larger displacement amplitudes. However, at the bottom of tunnel, the increase in tunnel thickness is accompanied by a rather large reduction in displacement amplitude.

c - The effect of bedrock depth is similar to the case without a tunnel structure, i.e., the primary resonance peak increases as the bedrock depth increases.

d - For a soil layer resting on a bedrock, the primary resonance frequency of the soil layer increases as the soil elastic modulus increases. Meanwhile, higher ground vibrations will be introduced by softer soil layers.

Acknowledgement

The research reported herein was sponsored in part by the National Science Council of the R.O.C. through the Grant No. NSC 92-2211-E-002-001.

References

Andersen, L. and Jones, C.J.C. (2006), "Coupled boundary and finite element analysis of vibration from railway tunnels-a comparison of two- and three-dimensional models", *J. Sound Vib.*, **293**, 611-625.

Balendra, T., Chua, K.H., Lo, K.W. and Lee, S.L. (1989), "Steady-state vibration of subway-soil-building system", ASCE *J. Eng. Mech.*, **115**(1), 145-162.

Balendra, T., Koh, C.G. and Ho, Y.C. (1991), "Dynamic Response of buildings due to trains in underground tunnels", *Earth. Eng. Struct. Dyn.*, **20**, 275-291.

Chatterjee, P., Degrande, G., Jacobs, S., Charlier, J., Bouvet, P. and Brassenx, D. (2003), "Experimental results of free field and structural vibrations due to underground railway traffic", *Tenth International Congress on Sound and Vibration*, 7-10 July, Stockholm, Sweden.

Chua, K.H., Lo, K.W. and Balendra, T. (1995), "Building response due to subway train traffic", ASCE *J. Geot. Eng.*, **121**(11), 747-754.

Clouteau, D., Arnst, M., Al-Hussaini, T.M. and Degrande, G. (2005), "Freefield vibrations due to dynamic loading on a tunnel embedded in a stratified medium", *J. Sound Vib.*, **283**, 173-199.

Degrande, G., Schevenels, M., Chatterjee, P., Van de Velde, W., Hölscher, P, Hopman, V., Wang, A., and Dadkah, N. (2006), "Vibration due to a test train at variable speeds in a deep bored tunnel embedded in london clay", *J. Sound Vib.*, **293**, 626-644.

Degrande, G., Clouteau, D., Othman, R., Arnst, M., Chebli, H., Klein, R., Chatterjee, P. and Janssens, B. (2006), "A numerical model for ground-borne vibrations from underground railway traffic based on a

periodic finite element-boundary element formulation", *J. Sound Vib.*, **29**3, 645-666.
Forrest, J.A. and Hunt, H.E.M. (2006a), "A three-dimensional tunnel model for calculation of train-induced ground vibration." *J. Sound Vib.*, **294**, 678-705.
Forrest, J.A. and Hunt, H.E.M. (2006b), "Ground vibration generated by trains in underground tunnels", *J. Sound Vib.*, **294**, 706-736.
Gardien, W. and Stuit, H.G.. (2003), "Modelling of soil vibrations from railway tunnels", *J. Sound Vib.*, **267**, 605-619.
Hood, R.A., Greer, R.J., Breslin, M. and Williams, P.R. (1996), "The calculation and assessment of ground-borne noise and perceptible vibration from trains in tunnels", *J. Sound Vib.*, **193**(1), 215-225.
Kurzweil, L.G. (1979), "Ground-borne noise and vibration from underground rail systems", *J. Sound Vib.*, **66**(3), 363-370.
Melke, J. (1988), "Noise and vibration from underground railway lines: proposals for a prediction procedure", *J. Sound Vib.*, **120**(2), 391-406.
Metrikine, A.V. and Vrouwenvelder, A.C.W.M. (2000), "Surface ground vibration due to moving train in a tunnel: two-dimensional model", *J. Sound Vib.* **234**(1), 43-66.
Thiede, R. and Natke, H.G. (1991), "The influence of thickness variation of subway walls on the vibration emission generated by subway traffic", *Soil Dyn Earthquake Eng V: Int. Conf Soil Dyn Earthquake Eng,* Computational Mechanics Publications, Southampton, UK, 673-682.
Trochides, A. (1991), "Ground-borne vibrations in buildings near subways", *Appl. Acoustics*, **32**, 289-296.
Pan, C.S. and Xie, Z.G. (1990), "Measurement and analysis of vibrations caused by passing trains in subway running tunnel", *China Civil Eng. J.*, **23**(2):21-28 (in Chinese).
Yang, Y.B., Kuo, S.R. and Hung, H.H. (1996), "Frequency-independent infinite element for analyzing semi-infinite problems", *Int. J. Num. Meth. Eng.*, **39**, 3553-3569.
Yang, Y.B. and Hung, H.H. (2001), "A 2.5D finite/infinite element approach for modeling visco-elastic bodies subjected to moving loads", *Int. J. Num. Meth. Eng.*, **51**, 1317-1336.
Wolf, J.P. (1985), *Dynamic Soil-Structure Interaction*. Englewood Cliffs, NJ: Prentice-Hall.